S O L A R   C Y C L E   24   A S   S E E N   B Y   S D O

A New Sigmoid Catalog from *Hinode* and the *Solar Dynamics Observatory*: Statistical Properties and Evolutionary Histories

**A.S. Savcheva · S.C. McKillop · P.I. McCauley ·
E.M. Hanson · E.E. DeLuca**

Abstract We present a new sigmoid catalog covering the duration of the *Hinode* mission and the *Solar Dynamics Observatory* (SDO) until the end of 2012. The catalog consists of 72 mostly *long-lasting* sigmoids. We collect and make available all X-ray and EUV data from *Hinode*, SDO, and the *Solar TErrestrial RElations Observatory* (STEREO), and we determine the sigmoid lifetimes, sizes, and aspect ratios. We also collect the line-of-sight magnetograms from the *Helioseismic and Magnetic Imager* (HMI) for SDO or the *Michelson Doppler Imager* (MDI) on the *Solar and Heliospheric Observatory* (SOHO) to measure flux *versus* time for the lifetime of each region. We determine that the development of a sigmoidal shape and eruptive activity is more strongly correlated with flux cancelation than with emergence. We find that the eruptive properties of the regions correlate well with the maximum flux, largest change, and net change in flux in the regions. These results have implications for constraining future flux-rope models of ARs and gaining insight into their evolutionary properties.

1. Introduction

S-shaped ARs were observed first with the *Yohkoh* satellite (Acton *et al.*, 1992) and later termed sigmoids by Rust and Kumar (1996). The first statistical study by Rust and Kumar (1996) utilizing several years of *Yohkoh* data, showed the presence of transient sigmoids

---

A.S. Savcheva (✉) · S.C. McKillop · P.I. McCauley · E.E. DeLuca
Harvard-Smithsonian Center for Astrophysics, 60 Garden St., Cambridge, MA 02138, USA
e-mail: asavcheva@cfa.harvard.edu

E.M. Hanson
Department of Physics, University of California, 366 LeConte Hall #7300, Berkeley, CA 94720-7300, USA

ⓐ Springer

(present for less than 12 hours before eruptions). Later, Canfield, Hudson, and McKenzie (1999) and Canfield *et al.* (2007) performed a more thorough statistical investigation of the eruption frequency of these regions, showing that 83 % of sigmoids produce CMEs observed by *Large Angle and Spectrometric Coronagraph Experiment* (LASCO) on the *Solar and Heliospheric Observatory* (SOHO) and that they are 67 % more likely to erupt than non-sigmoidal regions. This unambiguous association of sigmoids as precursors to solar eruptions motivated multiple authors to study them in great detail observationally and to base analytical and numerical models on the appearance of sigmoids. Comparing magnetogram and X-ray images shows that the spine of the sigmoid crosses the polarity inversion line (PIL) from the negative to the positive direction, indicating the presence of a flux rope underlying the sigmoid (Green and Kliem, 2009). Thus, sigmoids have traditionally been modeled as flux ropes in a potential arcade (Titov and Démoulin, 1999; Amari *et al.*, 2000; Török, Kliem, and Titov, 2004; Fan and Gibson, 2004; Aulanier *et al.*, 2010).

Multiple authors have analyzed the characteristics, appearance, and evolution of individual sigmoids either by thorough observational analysis (Sterling *et al.*, 2000; Glover *et al.*, 2001; Gibson *et al.*, 2002; Green and Kliem, 2009; Tripathi *et al.*, 2009; Green, Kliem, and Wallace, 2011) or in the context of their 3D magnetic-field structure obtained either from simulations (Amari *et al.*, 2000; Fan and Gibson, 2004; Török, Kliem, and Titov, 2004; Gibson and Fan, 2006; Aulanier *et al.*, 2010) or magnetic models and extrapolations (Régnier and Amari, 2004; Savcheva and van Ballegooijen, 2009; Savcheva, van Ballegooijen, and DeLuca, 2012; Savcheva *et al.*, 2012a, 2012b). The detailed analyses presented in these articles can only be performed on a limited number of sigmoids. In particular, magnetic extrapolations of sigmoids constrained by observations are static and time-consuming: limiting the number of cases that can be done.

The major questions about sigmoids are how the flux ropes form and how they destabilize to produce an eruption. There are three leading models for the formation of the flux ropes that comprise active-region (AR) sigmoids: flux cancelation at the PIL (van Ballegooijen and Martens, 1989), twisting of the leading and following AR polarities (Amari *et al.*, 2000; Aulanier *et al.*, 2010), or by emergence through the photosphere (Fan, 2001). The observational support for flux-rope formation by twisting motions is limited (Kazachenko *et al.*, 2010), although it is often used in simulations and models. Flux cancelation is thought to produce mainly *long-lasting* sigmoids (visible for days or weeks), and flux emergence may be associated more with short-lived sigmoids due to their more abrupt and dynamical nature.

We can gain significant insight into the questions of formation and destabilization by looking at the evolution and physical properties of observed sigmoids. In this article, we derive the physical properties of 72 sigmoids observed by the *X-ray Telescope* (XRT: Golub *et al.*, 2007) onboard *Hinode* and the *Atmospheric Imaging Assembly* (AIA: Lemen *et al.*, 2012) onboard the *Solar Dynamics Observatory* (SDO: Pesnell, Thompson, and Chamberlin, 2012). Although sigmoids were widely observed with the *Soft X-ray Telescope* (SXT) onboard *Yohkoh*, and a database of *Yohkoh* sigmoids exists, a systematic analysis of their observed properties has never been performed aside from eruption statistics (Rust and Kumar, 1996; Canfield, Hudson, and McKenzie, 1999; Canfield *et al.*, 2007). SXT's spatial resolution was $2.5 - 9$ times lower than current X-ray observations with XRT ($1''$) and even lower than the coronal observations made with SDO/AIA ($0.6''$). Our catalog utilizes the outstanding temporal coverage of AIA to track the evolution of the sigmoids and the associated magnetograms from the *Helioseismic and Magnetic Imager* for SDO (HMI: Schou *et al.*, 2012). The catalog covers the period from *Hinode* launch in 2006 to the end of 2012. It will be useful to scientists interested in finding datasets for more detailed studies and for comparison with the automated sigmoid sniffer from the AIA feature-finding team (Martens *et al.*, 2012).

In this article, we give an observational overview of sigmoids and address questions about their formation, evolution, and eruption. The article is organized as follows: In Section 2, we present our selection criteria and data-collection procedure for the catalog. In Section 3, we describe the sigmoid catalog and show the statistical properties derived from it. In Section 4, we present an analysis of the magnetic-flux evolution in conjunction with the eruptive behavior in the sample, and we describe what implications this might have for a consistent picture of sigmoid formation and eruption mechanisms. In Section 5, we give the conclusions of this work.

2. Collection of Observations

The first step in assembling this catalog was to select all sigmoid events for the duration of the *Hinode* and SDO missions until 2013. Since the sigmoidal shape is most prominent in soft X-rays, we used a mission-long XRT movie composed of full-disk images in the Ti/poly filter with cadence of 6 – 12 hours to select most regions. When XRT data were not available, we used full-disk monthly movies from AIA in the 335 Å channel with a 0.5-hour cadence. The AIA 335 Å passband has a high-temperature contribution that peaks at about 2.5 MK and a cooler contribution from 1 MK and below. Of all AIA passbands, 335 Å looks the most similar to XRT in AR cores. We include only AR sigmoids that have a definite S or double-J shape composed of multiple loops, excluding any AR interconnecting loops or transequatorial loops. Due to our selection methods, the catalog is biased toward *long-lasting* sigmoids, although a few transient ones were included, mainly in large complex regions.

We selected 72 sigmoids, which we gave a rating (between 0 and 4) based on the prominence of the S-shape and the appropriateness of the region for further studies. This measure is highly subjective, and so we refrain from using it in the statistical analysis. It is, however, useful for researchers seeking to study well-formed sigmoids in detail. A selection of sigmoids is shown in Figure 1.

For all regions, we collect the following available data:

- X-ray and EUV data from XRT and AIA. Before the launch of SDO: data from STEREO is useful for identifying filaments, although STEREO passbands are too cool to observe the hot sigmoidal loops.
- Magnetic-field data from SDO/HMI or SOHO/MDI prior to SDO launch
- Hα data from Kanzelhöhe or GONG, depending on the availability on www.solarmonitor.org.
- Screen shots from www.solar.monitor.com that show the full disk with marked NOAA region numbers.
- Flare peak time and GOES class are taken from the NOAA database (www.swpc.noaa.gov/ftpdir/indices/events/).
- CMEs from SOHO/LASCO taken from the CACTus database (www.sidc.oma.be/cactus/).

We make movies of all high-cadence data. The AIA movies follow the region from its appearance to its disappearance on the disk. In addition, we make high-cadence (30 seconds) movies for each flare observed with AIA in these regions, starting two hours before and ending two hours after the end of the flares. Inspection of these movies provides insight into the flare process and helps to identify suitable flaring regions for further case studies. The magnetogram data are full-disk and useful for determining how the flux is distributed in the region, *i.e.* a simple bipolar configuration or more complex. Partial magnetograms are used
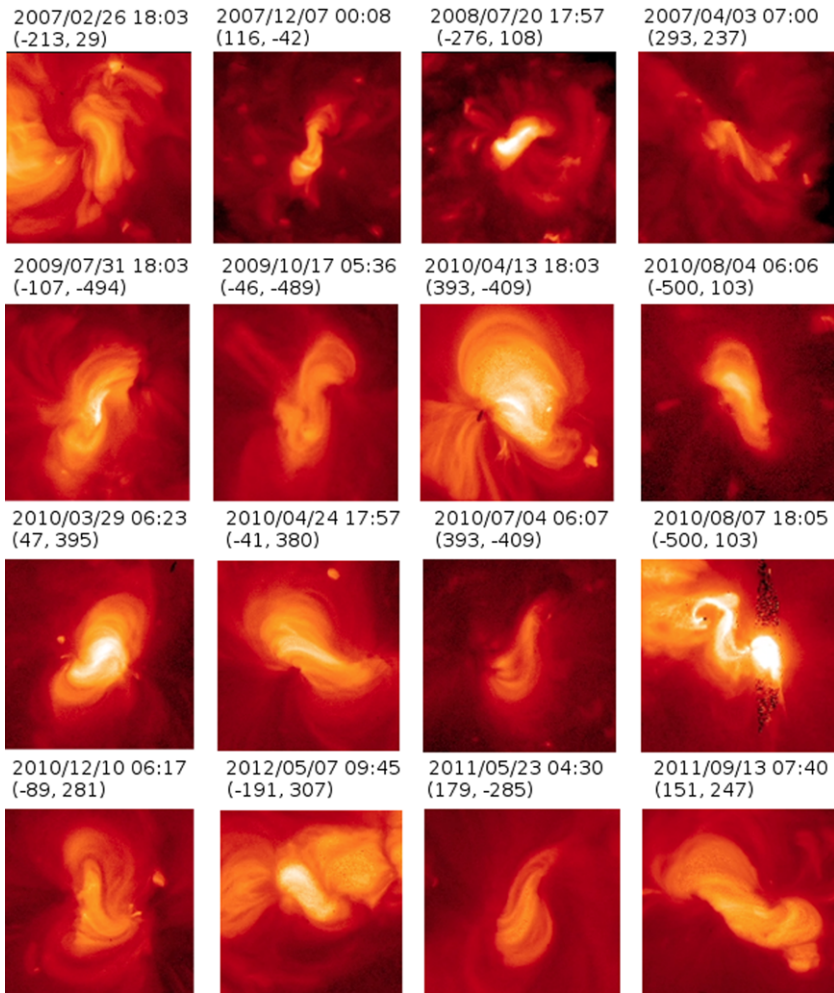
Figure 1 A collection of sigmoid cutout images from *Hinode*/XRT in the Ti/poly filter. Some of the sigmoids are S-shaped and some have an inverted-S shape. These sigmoids vary in size and the field of view of all images is the same – $256'' \times 256''$. The time and center of the field of view in arcsec are given above the images.

further in this analysis for measuring the magnetic flux over the lifetime of the regions (see Section 3).

We also note the presence of several potentially interesting features such as filaments, coronal holes, and post-flare loops. See Table 1 for a full listing of the features that we cataloged.

3. Statistics with the New Sigmoid Catalog

The catalog consists of two parts: Collections of basic observational information and the determination of the various parameters listed in Table 1. In the following subsec-

tions, we describe how each parameter was determined along with their associated statistical results. The online catalog is hosted at the Smithsonian Astrophysical Observatory at aia.cfa.harvard.edu/sigmoid.shtml. It is linked to the XRT mission-long flare catalog (xrt.cfa.harvard.edu/flare_catalog/). We will continue updating the web catalog until we complete the current solar cycle and will add more functionality per requests from the community.

3.1. Sigmoid Lifetime

We identify the times when the region hosting the sigmoid appears and disappears from the solar disk from inspection of the XRT and AIA movies. In most cases, the sigmoids form in regions that are seen to cross the entire disk of the Sun. These regions are observed for about two weeks and the sigmoidal shape is observed for only a portion of that time. Often, our selection criteria do not allow us to distinguish the sigmoidal shape when the regions are far from the central meridian, due to projection effects in the optically thin loops. One could potentially use STEREO to mitigate this effect, but we leave this to future case studies.

We show a histogram of the sigmoid lifetimes (the period over which a sigmoidal shape is present) in the lower-right panel of Figure 2. Sigmoids have a large spread in lifetimes, but most last for $2 - 2.5$ days, which is a relatively short time compared to the lifetime of the host regions. This is probably not a selection effect since a clear sigmoidal shape can usually be distinguished for more than a week around the central meridian. If sigmoids are taken as direct observational evidence of flux ropes (Green, Kliem, and Wallace, 2011), this means that the flux ropes also survive for just $2 - 3$ days. The sigmoid disappears either as a result of an eruption (sometimes causing a CME or sometimes a failed eruption) or as a result of decay in the supporting fields. Sigmoids are disrupted by eruption in one-third of the cases that show flares. This statistical result (based on 72 regions) might be important for constraining future global simulations containing ARs with flux ropes, which require information about the lifetime and evolution of the flux ropes.

3.2. Hemispheric Rule

We record whether the sigmoid is S-shaped or an inverted S and in which hemisphere it is observed. This information helps us to confirm the hemispheric rule for sigmoids (Zirker *et al.*, 1997; Pevtsov, Canfield, and Latushko, 2001), which states that sigmoids in the Northern hemisphere are predominantly an inverted S, and those in the South are a straight S. Sigmoids in the South are composed of predominantly right-bearing loops with positive helicity, and those in the North consist of left-bearing loops with negative helicity (Canfield *et al.*, 2007). From our statistical study, we determine that 88 % of the sigmoids in the North have an inverted S-shape, and 78 % of the ones in the South are straight S-shaped, which shows a stronger hemispheric rule than previous results (Canfield, Hudson, and McKenzie, 1999). The exceptions to this rule come mostly from complex ARs that have multiple inversion lines and not a simple leading/trailing polarity configuration. Or, in a limited number of cases, they come from sigmoids that appear right at the Equator and are aligned with it.

In our sample, most of the sigmoids appear in the southern hemisphere (46) *versus* only 25 in the North. This uneven distribution is likely related to hemispheric phasing of the solar cycle, but more needs to be done to understand the origin of this effect. The results of the automatic sigmoid detection in AIA provided by the AIA Feature Finding Team's sigmoid sniffer on the Heliophysics Events Knowledgebase (HEK) can be used to test our selection methods when the implementation of the feature tracker is complete.

Table 1 A compilation of the sigmoid parameters recorded in our catalog.

| Parameter	Units	Example
Sigmoid ID	–	S65
Rating	–	3
NOAA AR	–	11471
AR start date (when region appears on disk)	YYYY.MM.DD	2012.04.27
AR start time	HH:MM	17:00
AR end date (when region disappears on disk)	YYYY.MM.DD	2012.05.11
AR end time	HH:MM	11:00
Sigmoid start date (when S-shape develops)	YYYY.MM.DD	2012.05.04
Sigmoid start time	HH:MM	05:30
Sigmoid end date (when S-shape disappears)	YYYY.MM.DD	2012.05.09
Sigmoid end date	HH:MM	15:30
Peak sigmoid date (when sigmoid is most prominent)	YYYY.MM.DD	2012.05.05
Peak sigmoid time	HH:MM	12:00
X-coordinate (from Sun center at peak sigmoid time)	Arcsec	176
Y-coordinate (from Sun center at peak sigmoid time)	Arcsec	-303
Lifetime	Days	5.4
Straight/Inverted S	–	S
Hemisphere	–	S
Size (along long axis)	Arcsec	230
Aspect ratio	–	2.7
EUV Filament?	–	Yes
Hα filament?	–	Yes
Sunspots (number)	–	Yes, multiple
Flux emergence	–	Yes
Flux cancelation	–	Yes
Peak flux	$\times 10^{21}$ Mx	16
Flare date	YYYY.MM.DD	2012.04.30
Peak flare time	HH:MM	02:53
Flare class (from GOES)	–	C2.4
CME start time	YYYY.MM.DD HH:MM	
CME duration	–	
Filament eruption	–	None
Transient coronal holes	–	None
Flare ribbons	–	No
Post-flare loops	–	No
Nearby coronal holes	–	Yes
Nearby ARs	–	AR 11470, 11472
XRT frames	–	
XRT synoptic	–	Yes
Comments	–	
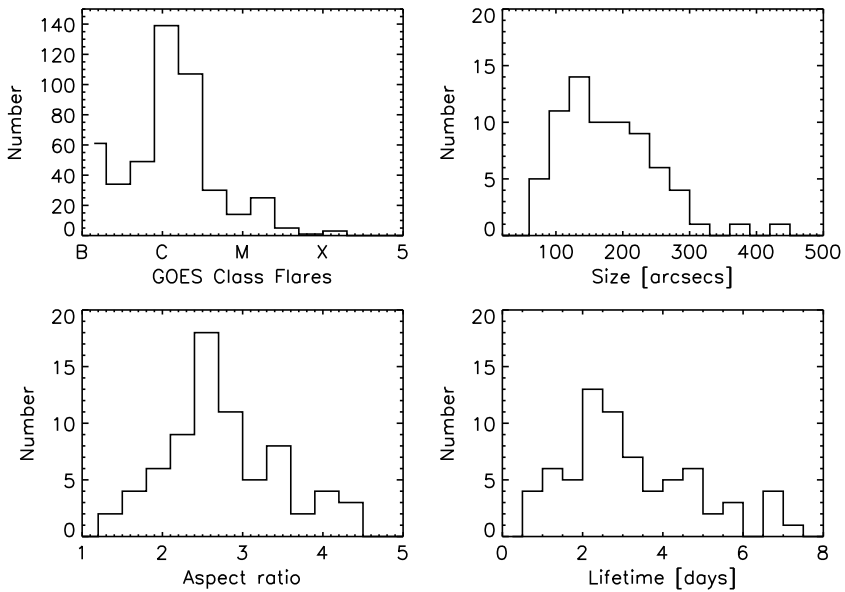
Figure 2 Histograms of parameters measured in the sigmoid catalog.

3.3. Sizes

We measure the approximate size of the sigmoids by scaling all images equally and manually selecting the extent of the elbows of the sigmoids. In the upper-right of Figure 2, we show a histogram of the sizes of all 72 sigmoids. The distribution peaks at about $130''$ and is relatively broad. There are a large number of small sigmoids, mostly with rating below 3. The far end of the distribution, toward larger sizes, is due to the presence of large quiescent-Sun (large dispersed polarities) sigmoids, associated with long faint loops, appearing as fuzzy emission in XRT.

We measure the ratio of the long to short axes of the sigmoid to compute the aspect ratio. In the lower-left panel of the figure, we have plotted the histogram of the aspect ratio, which peaks prominently at 2.5. This result has implications for constraining sigmoid models. For example, Aulanier *et al.* (2010) produce a very thin sigmoid in their MHD simulation, which has a very large aspect ratio. This is achieved by making a very thin shear layer between two rotating polarities. Our result is an indication that the shearing layer in such a simulation should be thicker or that another mechanism is at work since much thicker sigmoids are observed.

3.4. Eruptivity

Another important characteristic of sigmoids is their high eruption rate. Studies of the flaring and CME-producing activity of sigmoids observed with *Yohkoh*/SXT have been conducted in the past (Canfield, Hudson, and McKenzie, 1999; Canfield *et al.*, 2007). In this study we confirm their result: we find that 64 % of the sigmoids produce GOES-class flares. However, GOES does not always detect all flares in a region. For example, inspection of the AIA movies found about ten additional flares that were not classified by GOES. The distribution of the GOES classes for the observed flares is shown in Figure 2: the distribution

has a noticeable peak in early C-class. An inspection of the catalog would show that earlier, before the launch of SDO, most flares were B-class since they appeared earlier in the solar cycle, and after 2010 a significant number of C-class flares appear producing the tail in the distribution.

We find that most of the regions that produce flares produce more than one flare: 49 % of the total number of sigmoids or 76 % of the flare-producing sigmoids. We determine that the lifetime of the regions that produce more than one flare is increased from the mean value of 2.5 to 3.8 days, which is not surprising since energy has to build up in between events. The average size of the sigmoids producing more than one flare is also higher than the peak of the histogram: 210″. This is also not surprising since more complex regions tend to display this behavior, and they are generally larger. We have a very high association rate of flares with CMEs (89 %).

3.5. Filaments and Sigmoids

Sigmoids are thought to be associated with filaments most of the time, so we test this assumption. We can determine the association with filaments unambiguously only for 54 regions from looking at the Hα images. We find that 35 of them (65 %) are associated with Hα filaments that run parallel to the PIL, and 19 are not. Out of the 42 regions, for which we can unambiguously determine the presence of EUV filaments, 14 (33 %) have EUV filaments and 28 do not. These percentages seem relatively low given the idea that the filament is visible due to emitting material collected in the dips of the flux-rope field lines. Some sigmoids that we selected for the catalog are in the stage of a sheared arcade, so it is possible that they are not associated with filaments. We plan a detailed study of the filaments in sigmoidal ARs to determine whether the filaments grow with time in the case when continual flux cancelation is observed as suggested by the standard flux-cancelation cartoon (van Ballegooijen and Martens, 1989). In this case we would be able to take advantage of the STEREO data that extends beyond the near-side of the Sun.

4. Magnetic Evolution and Sigmoid Evolutionary Histories

A major undertaking in this project is to obtain a comprehensive picture of the evolution of sigmoids. This is achieved on two fronts: utilizing the data described in the previous section on the shape, size, lifetime, and flare properties of the observed sigmoids in a large wavelength range; and by placing these observations in the context of the photospheric magnetic evolution of the regions. For this purpose we compose animated sequences of partial-disk magnetograms taken from SDO/HMI when available, and SOHO/MDI when not, centered on the region and tracking it as it crosses the solar disk. These movies show the evolution of the magnetic flux over the lifetime of the sigmoid-hosting regions. These movies can be used to gain insight into the dynamics in the particular region – the motion of particular magnetic-flux elements and the overall distribution of the flux.

4.1. Measuring the Magnetic Flux

We measure the magnetic flux in the regions over their lifetime, using LoS magnetograms covering the lifetime of the host regions with three-hour cadence. The measurements are from time-averaged 12-minute HMI and 96-minute MDI data. Although in this study LoS magnetograms give sufficient information, we note that when regions are far from disk center or include sunspots with strong horizontal fields, the full vector magnetograms should be

used. It is impractical to incorporate the analysis of thousands of vector magnetograms for survey purposes, so we encourage the use of vector magnetograms for specific case studies only. We aim at just enclosing the primary flux concentration in a square box (see the HMI and MDI movies in the catalog). The noise level in each magnetogram is determined using the method described by Thornton and Parnell (2011). All pixels below this level are discarded (Thornton and Parnell, 2011). In addition, to keep a pixel value as non-zero, we require that at least four of its eight neighbors all have the same sign. By keeping only the significant pixels as the region crosses the disk, the flux measurements from regions away from disk center are more reliable.

We correct for area foreshortening by dividing the area of the pixel by $\cos\theta$, where θ is the angular distance from disk center. Another $\cos\theta$ correction is needed to correct for the fact that away from disk center the line-of-sight (LoS) magnetic field (which is measured in the magnetograms) deviates from the radial magnetic field. This way we effectively derotate all partial magnetograms to disk center. The flux in the region is determined by

$$F = \sum_{i=0}^{n} B_{\text{LoS},i} a \frac{1}{\cos\theta_i^2}, \tag{1}$$

where a is the physical area of a single pixel at disk center for the given time of observation, and $B_{\text{LoS},i}$ is the magnetic field as measured from the magnetogram for a given pixel. We compute F separately for the positive and negative polarity. We disregard the eastmost and westmost few magnetograms when the regions are close to the limb, since there our corrections reach their limits and very often the bounding box includes other regions that appear in projection close to the region of interest. Generally, for the more noisy MDI data, we only measured the fluxes within 50° of disk center, and for HMI within 60°. For all sigmoids in the catalog, we plot the value of the flux [F] in time and look for signs of decreasing (flux cancelation) or increasing flux (flux emergence). In Figure 3, we have shown examples of four such magnetic-flux evolution plots. One plot shows basically unchanging flux, one shows emergence and then cancelation, one shows only cancelation, and one only emergence. Such plots accompany the magnetogram movies in the online catalog.

4.2. Formation Mechanism

We aim to determine which mechanism is dominant for producing sigmoids: flux cancelation or emergence. The large complex regions usually display flux emergence or combination of emergence and cancelation. We have a large number of smaller and fainter regions, which, percentage-wise, display more flux cancelation or relatively constant flux. We determine that 57 % of the sigmoids show definite cancelation (more than the noise in the flux curves) and 35 % show emergence. The rest do not show much evolution in the flux. In 50 % of the cases, the sigmoid shape is observed during the flux-cancelation episode and 19 % during emergence. Based on this result, we conclude that flux cancelation is the dominant process for the production of sigmoids. The flux-cancelation picture (van Ballegooijen and Martens, 1989) points to the fact that flux cancelation can build *long-lasting* sigmoids, which our catalog is biased toward. Savcheva *et al.* (2012a) show how flux cancelation in three sigmoids influence the building the S-shape by means of data-driven magnetic modeling. However, here, for the first time we show observationally that flux cancelation plays a vital role in the development and eruptive behavior of sigmoids by looking at a statistically significant sample.
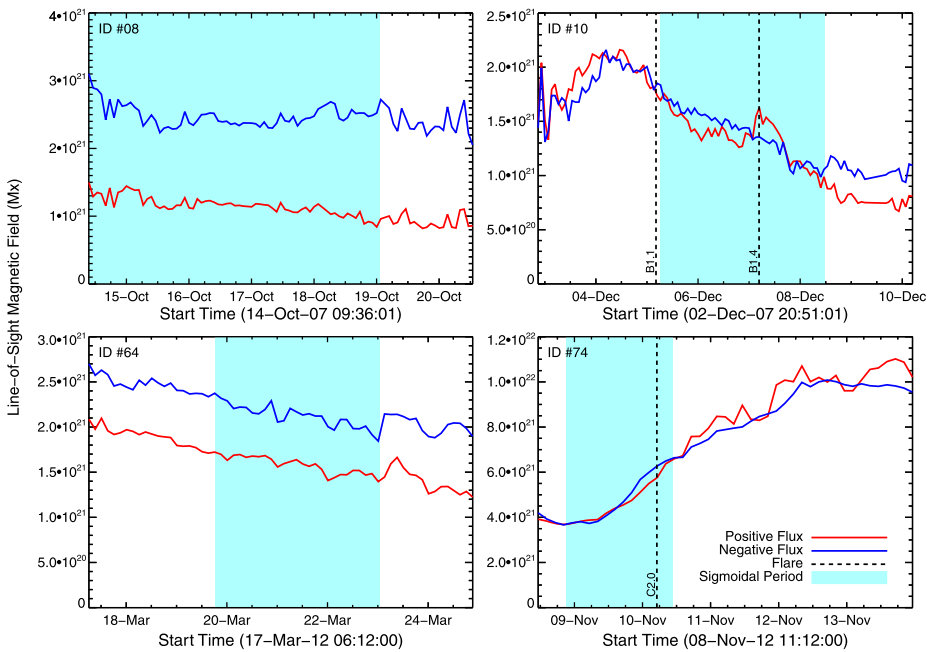
Figure 3 Four examples of magnetic-flux measurements with time for the whole lifetime of the regions. ID 10 and 64 show clear flux cancelation (decreasing flux with time) for sigmoids, 10 shows emergence followed by cancelation, and 74 shows only emergence. ID 08 shows neither cancelation nor emergence The dashed lines mark the flare times, and the blue shaded regions mark when sigmoid shape is observed.

4.3. Eruptive Properties and Magnetic Flux Evolution

We mark the times of the flares (dashed lines) and the period when sigmoid shape is observed (blue shaded region) on all flux plots as in Figure 3, so we can put them in relation with each other. We aim at studying when flares appear with respect to flux-cancelation or -emergence episodes. We find that for 26 flares, the sigmoid shape remains intact after the flare, meaning that in 26 cases out of about 250, the sigmoid reforms after the flare (or survives the flare) and continues evolving. 100 flares are observed during flux cancelation, and 118 during emergence, which is an insignificant difference. This result is not surprising since emergence is a much more dynamic phenomenon which takes place at much larger scales and involves larger portions of flux at a time. We also find that the largest flare in multi-flare regions appears with the same probability in the flux cancelation and emergence portions of the flux curve. These results have implications for ARs in general not only to sigmoidal eruptive activity.

We correlate the flux parameters with the number of flares and largest-flare GOES class in the regions as a proxy of peak X-ray flux. In Figure 4 we have shown three plots of such correlations that display a strong positive result. The correlation coefficients and the corresponding statistical significance, given by the *p*-value, are shown in Table 2. We find that larger number of flares are observed in regions with higher maximum flux, or rather the range of number of flares extends higher (Figure 4a). This can be explained by the fact that a larger region and/or region with stronger polarities contains more non-potential magnetic energy to power multiple flares. Similar results have been obtained before for ARs producing
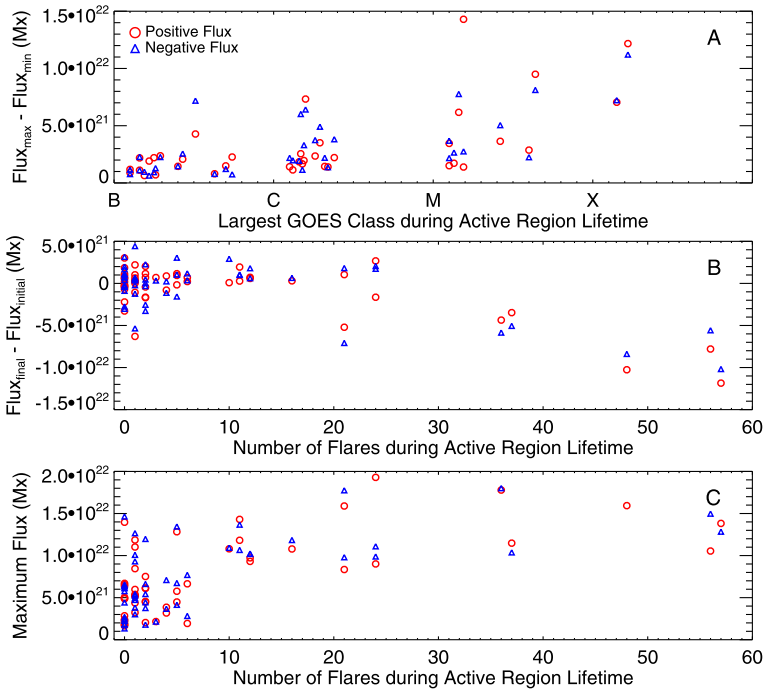
Figure 4 (a) Largest flare observed in a given region *versus* largest change in flux (maximum flux minus minimum flux) – there is a trend for the number of large flares to increase with increasing δF; (b) Number of flares in a region *versus* the net flux change over the observed period – there is a significant correlation between the number of flares and the value of the negative net flux, *i.e.* net flux cancelation; (c) The number of flares in a given AR *versus* the maximum flux measured in this region during its lifetime on the disk.

larger than C-class flares (Welsch *et al.*, 2009). We also find a correlation between the largest flare and the maximum flux, as indicated by Mayfield and Lawrence (1985). The largest flare in a region correlates well with the largest change in flux ($\delta F = F_{max} - F_{min}$), which is also logical since larger δF means more dynamics in the region and hence potentially more chances for destabilization of the magnetic configuration. The strongest correlation is found between the number of flares in a region and the net flux change over their lifetime, which is strongly skewed towards flux cancelation. This result again points to the role of flux cancelation in the evolution process in these regions. When comparing the flare statistics in sigmoidal ARs with overall AR flare statistics, it is important to keep in mind that our selection criteria preferentially select long-lived and decaying ARs, as these are the regions in which sigmoids tend to form. Young, dynamic erupting AR are not generally included in the catalog for this reason. Thus, our flare statistics need to be used in the context of understanding energy storage and release in sigmoidal systems.

5. Conclusions

We present here the compilation and first statistical analysis of a sigmoid catalog covering the duration of the *Hinode* and SDO missions. It consists of data for 72 sigmoids that appeared on the Sun from December 2006 to December 2012. Such catalogs with data, but

Table 2 Linear Pierson correlation coefficient and *p*-values.

Quantities	Polarity	R	p
Largest flare – Maximum flux	+	0.67	4.5×10^{-8}
	−	0.6	7.7×10^{-8}
Number of flares – Maximum flux*	+	0.64	3.4×10^{-7}
	−	0.68	3.7×10^{-8}
Largest flare – δF*	+	0.51	1.1×10^{-4}
	−	0.53	5.1×10^{-5}
Number of flares – δF	+	0.78	7.0×10^{-12}
	−	0.74	3.4×10^{-10}
Largest flare – Net change in flux	+	−0.43	1.5×10^{-3}
	−	−0.38	5.7×10^{-3}
Number of flares – Net change in flux*	+	−0.73	1.1×10^{-9}
	−	−0.64	4.2×10^{-7}

The correlations with asterisks are plotted in Figure 4.

without the measured sigmoid properties, exist for the *Yohkoh* era. Canfield, Hudson, and McKenzie (1999), Canfield *et al.* (2007) and Glover *et al.* (2001) have used them to derive the eruption rate in sigmoids. The present catalog is more comprehensive, covering the appearance of the sigmoids in all layers of the atmosphere – from the photosphere to the far corona (during CMEs). We measure a large set of parameters. The mean values and the scatter in these parameters can be potentially useful for constraining global models of flux-rope evolution such as the ones by Yeates, Mackay, and van Ballegooijen (2008). The breadth of the datasets featured for each sigmoid can be potentially very useful for selecting events for future case studies.

The main results from this work are listed below:

i) Sigmoid lifetimes: Distribution peaks at $2 - 2.5$ days (Section 3.1).
ii) Hemispheric rule: 88 % of the sigmoids in the North are inverted S-shape, and 78 % of the sigmoids in the South are S-shaped (Section 3.2).
iii) Sizes: Peak at $130''$ for all regions and $210''$ for regions that flare more than once (Section 3.5).
iv) Eruptivity: 64 % of the sigmoidal regions produce flares, 49 % produce more than one flare (Section 3.4), which confirms the results of Canfield, Hudson, and McKenzie (1999) and Canfield *et al.* (2007).
v) Filaments: 65 % of the sigmoids are associated with Hα filaments and 33 % with EUV filaments (Section 3.5).

In addition, we create a set of evolutionary histories for each sigmoid. This is done by measuring the LoS photospheric flux in a region enclosing the sigmoid and following its evolution over the lifetime of the sigmoid-hosting region. Over each flux curve, we plot the period when the S-shape is present and the timing of flares with their respective GOES classes. Putting these events in the context of magnetic-flux evolution, we conclude that:

vi) The sigmoids in our catalog are predominantly formed and evolve in response to flux cancelation: 57 % *vs.* 35 %. The sigmoidal shape appears mostly during flux cancelation – in 50 % of the cases, and during emergence in 19 % of the cases. Even during a large flux-emergence event, a flux rope may be formed post-factum in the corona from the

converging flows toward the PIL that the emergence creates, which gives conditions for flux cancelation at the PIL during the emergence event (Section 4.2).

vii) Flares are produced almost equally during flux-cancelation and -emergence events (Section 4.3).

viii) We find strong correlation between the flaring activity and the flux amplitude in the regions (Section 4.3).

These results have large implications for understanding the formation, evolution, and eruption of sigmoidal regions and the eruptive behavior of solar ARs in general. They point to the fact that flux cancelation plays a more important role in sigmoid development and eruption frequency than flux emergence, which is especially useful for directing the attention of the community to this mechanism.

References

Acton, L., Tsuneta, S., Ogawara, Y., Bentley, R., Bruner, M., Canfield, R., Culhane, L., Doschek, G., Hiei, E., Hirayama, T., Hudson, H., Kosugi, T., Lang, J., Lemen, J., Nishimura, J., Makishima, K., Uchida, Y., Watanabe, T.: 1992, The YOHKOH mission for high-energy solar physics. *Science* **258**, 591. ADS.

Amari, T., Luciani, J.F., Mikic, Z., Linker, J.: 2000, A twisted flux rope model for coronal mass ejections and two-ribbon flares. *Astrophys. J. Lett.* **529**, L49.

Aulanier, G., Török, T., Démoulin, P., DeLuca, E.E.: 2010, Formation of torus-unstable flux ropes and electric currents in erupting sigmoids. *Astrophys. J.* **708**, 314.

Canfield, R.C., Hudson, H.S., McKenzie, D.E.: 1999, Sigmoidal morphology and eruptive solar activity. *Geophys. Res. Lett.* **26**, 627.

Canfield, R.C., Kazachenko, M.D., Acton, L.W., Mackay, D.H., Son, J., Freeman, T.L.: 2007, Yohkoh SXT full-resolution observations of sigmoids: Structure, formation, and eruption. *Astrophys. J. Lett.* **671**, L81.

Fan, Y.: 2001, The emergence of a twisted Ω-tube into the solar atmosphere. *Astrophys. J. Lett.* **554**, L111. ADS, DOI.

Fan, Y., Gibson, S.E.: 2004, Numerical simulations of three-dimensional coronal magnetic fields resulting from the emergence of twisted magnetic flux tubes. *Astrophys. J.* **609**, 1123.

Gibson, S.E., Fan, Y.: 2006, Coronal prominence structure and dynamics: A magnetic flux rope interpretation. *J. Geophys. Res.* **111**, 12103.

Gibson, S.E., Fletcher, L., Del Zanna, G., Pike, C.D., Mason, H.E., Mandrini, C.H., Démoulin, P., Gilbert, H., Burkepile, J., Holzer, T., Alexander, D., Liu, Y., Nitta, N., Qiu, J., Schmieder, B., Thompson, B.J.: 2002, The structure and evolution of a sigmoidal active region. *Astrophys. J.* **574**, 1021. ADS, DOI.

Glover, A., Harra, L.K., Matthews, S.A., Hori, K., Culhane, J.L.: 2001, Long term evolution of a non-active region sigmoid and its CME activity. *Astron. Astrophys.* **378**, 239. ADS, DOI.

Golub, L., DeLuca, E.E., Austin, G., Bookbinder, J., Caldwell, D., Cheimets, P., Cirtain, J., Cosmo, M., Reid, P., Sette, A., Weber, M., Sakao, T., Kano, R., Shibasaki, K., Hara, H., Tsuneta, S., Kumagai, K., Tamura, T., Shimojo, M., McCracken, J., Carpenter, J., Haight, H., Siler, R., Wright, E., Tucker, J., Rutledge, H., Barbera, M., Peres, G., Varisco, S.: 2007, The X-Ray Telescope (XRT) for the Hinode mission. *Solar Phys.* **243**, 63. ADS, DOI.

Green, L.M., Kliem, B.: 2009, Flux rope formation preceding coronal mass ejection onset. *Astrophys. J. Lett.* **700**, L83.

Green, L.M., Kliem, B., Wallace, A.J.: 2011, Photospheric flux cancellation and associated flux rope formation and eruption. *Astron. Astrophys.* **526**, 2.

Kazachenko, M.D., Canfield, R.C., Longcope, D.W., Qiu, J.: 2010, Sunspot rotation, flare energetics, and flux rope helicity: The Halloween flare on 2003 October 28. *Astrophys. J.* **722**, 1539. ADS, DOI.

Lemen, J.R., Title, A.M., Akin, D.J., Boerner, P.F., Chou, C., Drake, J.F., Duncan, D.W., Edwards, C.G., Friedlaender, F.M., Heyman, G.F., Hurlburt, N.E., Katz, N.L., Kushner, G.D., Levay, M., Lindgren, R.W., Mathur, D.P., McFeaters, E.L., Mitchell, S., Rehse, R.A., Schrijver, C.J., Springer, L.A., Stern, R.A., Tarbell, T.D., Wuelser, J.-P., Wolfson, C.J., Yanari, C., Bookbinder, J.A., Cheimets, P.N., Caldwell, D., Deluca, E.E., Gates, R., Golub, L., Park, S., Podgorski, W.A., Bush, R.I., Scherrer, P.H., Gummin, M.A., Smith, P., Auker, G., Jerram, P., Pool, P., Soufli, R., Windt, D.L., Beardsley, S., Clapp, M., Lang, J., Waltham, N.: 2012, *Solar Phys.* **275**, 17. ADS, DOI.

Martens, P.C.H., Attrill, G.D.R., Davey, A.R., Engell, A., Farid, S., Grigis, P.C., Kasper, J., Korreck, K., Saar, S.H., Savcheva, A., Su, Y., Testa, P., Wills-Davey, M., Bernasconi, P.N., Raouafi, N.-E., Delouille, V.A., Hochedez, J.F., Cirtain, J.W., Deforest, C.E., Angryk, R.A., de Moortel, I., Wiegelmann, T., Georgoulis, M.K., McAteer, R.T.J., Timmons, R.P.: 2012, Computer vision for the Solar Dynamics Observatory (SDO). *Solar Phys.* **275**, 79. ADS, DOI.

Mayfield, E.B.: Lawrence, J.K.: 1985, The correlation of solar flare production with magnetic energy in active regions, *Solar Phys.* **96**, 293. ADS, DOI.

Pesnell, W.D., Thompson, B.J., Chamberlin, P.C.: 2012, *Solar Phys.* **275**, 3. DOI.

Pevtsov, A.A., Canfield, R.C., Latushko, S.M.: 2001, Hemispheric helicity trend for solar cycle 23. *Astrophys. J. Lett.* **549**, L261. ADS, DOI.

Régnier, S., Amari, T.: 2004, 3D magnetic configuration of the Hα filament and X-ray sigmoid in NOAA AR 8151. *Astron. Astrophys.* **425**, 345. ADS, DOI.

Rust, D.M., Kumar, A.: 1996, Evidence for helically kinked magnetic flux ropes in solar eruptions. *Astrophys. J. Lett.* **464**, L199.

Savcheva, A., van Ballegooijen, A.: 2009, Nonlinear force-free modeling of a long-lasting coronal sigmoid. *Astrophys. J.* **703**, 1766.

Savcheva, A., van Ballegooijen, A.A., DeLuca, E.E.: 2012, Field topology analysis of a long-lasting coronal sigmoid. *Astrophys. J.* **744**, 78.

Savcheva, A.S., Green, L.M., van Ballegooijen, A.A., DeLuca, E.E.: 2012a, Photospheric flux cancellation and the build-up of sigmoidal flux ropes on the Sun. *Astrophys. J.* **759**, 105. ADS, DOI.

Savcheva, A., Pariat, E., van Ballegooijen, A., Aulanier, G., DeLuca, E.: 2012b, Sigmoidal active region on the Sun: Comparison of a magnetohydrodynamical simulation and a nonlinear force-free field model. *Astrophys. J.* **750**, 15. ADS, DOI.

Schou, J, Scherrer, P.H, Bush, R.I., Wachter, R., Couvidat, S., Rabello-Soares, M.C., Bogart, R.S., Hoeksema, J.T., Liu, Y., Duvall, T.L., Akin, D.J., Allard, B.A., Miles, J.W., Rairden, R., Shine, R.A., Tarbell, T.D., Title, A.M., Wolfson, C.J., Elmore, D.F., Norton, A.A., Tomczyk, S.: 2012, Design and ground calibration of the Helioseismic and Magnetic Imager (HMI) instrument on the Solar Dynamics Observatory (SDO). *Solar Phys.* **275**, 229. ADS, DOI.

Sterling, A.C., Hudson, H.S., Thompson, B.J., Zarro, D.M.: 2000, Yohkoh SXT and SOHO EIT observations of sigmoid-to-arcade evolution of structures associated with halo coronal mass ejections. *Astrophys. J.* **532**, 628. ADS, DOI.

Thornton, L.M., Parnell, C.E.: 2011, Small-scale flux emergence observed using Hinode/SOT. *Solar Phys.* **269**, 13. ADS, DOI.

Titov, V.S., Démoulin, P.: 1999, Basic topology of twisted magnetic configurations in solar flares. *Astron. Astrophys.* **351**, 707.

Török, T., Kliem, B., Titov, V.S.: 2004, Ideal kink instability of a magnetic loop equilibrium. *Astron. Astrophys.* **413**, L27.

Tripathi, D., Kliem, B., Mason, H.E., Young, P.R., Green, L.M.: 2009, Temperature tomography of a coronal sigmoid supporting the gradual formation of a flux rope. *Astrophys. J. Lett.* **698**, L27. ADS, DOI.

van Ballegooijen, A., Martens, P.C.H.: 1989, Formation and eruption of solar prominences. *Astrophys. J.* **343**, 971.

Welsch, B.T., Li, Y., Schuck, P.W., Fisher, G.H.: 2009, What is the relationship between photospheric flow fields and solar flares? *Astrophys. J.* **705**, 821. ADS, DOI.

Yeates, A.R., Mackay, D.H., van Ballegooijen, A.A.: 2008, Modelling the global solar corona II: Coronal evolution and filament chirality comparison. *Solar Phys.* **247**, 103. ADS, DOI.

Zirker, J.B., Martin, S.F., Harvey, K., Gaizauskas, V.: 1997, Global magnetic patterns of chirality. *Solar Phys.* **175**, 27. ADS, DOI.